

Research Article

Fabian Jakob*, Joshua Pollmeier and Hans-Peter Heim

Influences on the mechanical properties of SRCs in a combined compacting and back injecting process

<https://doi.org/10.1515/ipp-2021-4151>

Received July 4, 2021; accepted November 24, 2021;

published online March 3, 2022

Abstract: In this research paper, the effects of the combined compacting and back-injection process to produce back-injected self-reinforced composites on the mechanical properties of the self-reinforced composites (SRCs) are investigated. For this purpose, the parameters barrel temperature, time of injection and holding pressure were varied for the back injection. Tensile and bending tests were carried out on the SRCs. The results show that the mechanical properties depend to a large extent on the process parameters. The measured tensile strength varies between approx. 186 and 86 MPa, the stiffness between approx. 3500 and 2000 MPa. The flexural strength is measured between approx. 75 and 5 MPa, the flexural modulus between approx. 5480 and 650 MPa. Flexural tests are more suitable for evaluation of the consolidation, as tensile tests cannot evaluate the adhesion of the fabric layers to each other in the SRCs. Microscopic examinations show that consolidation by the back-injected melt can lead to smaller cross-sections in the SRCs compared to an area that was not back-injected. At high barrel temperatures, melting of individual fabric layers can occur, which explains, among other things, the drop in the mechanical properties of the SRCs.

Keywords: back-injection; hot compaction; self-reinforced; SRC; SR-PP.

1 Introduction

Self-reinforced composites (SRCs) are made up of a single polymer, contrary to conventional fibre composites. The embedded fibres and the matrix differ only through the

orientation of the macromolecular chains and the crystalline structures, and not through their fundamental chemical composition. SRCs are made from textile semi-finished products consisting of thermoplastic fibres, i.e. woven fabrics.

High-performance fibres made of polymers can attain very high strengths from 455 (PP) to 3100 MPa (UHMWPE) and stiffnesses from 0.5 (PP) to 170 GPa (UHMWPE) (Cherif 2011). These mechanical characteristics are attained through the macromolecular orientation and the directional crystalline structure within the fibres. The orientation in a preferred direction stresses the covalent bonds within the macromolecules, which can withstand higher forces due to their strength, resulting in a much higher strength and stiffness of the fibres. The orientation is initiated in the melt, fixed in the form of directed crystallisation through rapid cooling, and increased still further through subsequent stretching of the fibres in the entropy-elastic range. To produce SRCs, several layers of thermoplastic fabric are stacked and bonded to each other by means of heat and pressure in a hot compaction process. Hine and Ward et al. (Hine et al. 1993, 1998; Olley et al. 1993; Rasburn et al. 1995) were some of the first to use this hot compaction process. They first investigated the compaction parameters for round fibres, but after their initial experiments, switched to fabrics made of film strips or tapes, because the larger surface area of the tapes improves the adhesion of the fibres during hot compaction (Hine et al. 2003; Jordan et al. 2003; Le Bozec et al. 2000).

The production of SRCs is a temperature-sensitive process because of the thermoplastic fibres. The mechanical properties of the composite are dependent on the manufacturing parameters, since the orientation and the directional crystalline regions within the fibres are completely lost during melting, which also means that the good mechanical properties are lost. In the hot compaction process, the morphology and thus the mechanical properties of the SRCs can be influenced as a function of the process parameters (Biermann et al. 2015; Heim et al. 2012, 2013; Ries 2021).

*Corresponding author: Fabian Jakob, IfW Plastics Technology, University of Kassel, Mönchebergstrasse 3, 34125 Kassel, Germany, E-mail: jakob@uni-kassel.de

Joshua Pollmeier and Hans-Peter Heim, IfW Plastics Technology, University of Kassel, Kassel, Germany

SRCs differ decisively in this aspect from thermoplastics reinforced with foreign fibres (e.g. organo sheets), in which the fibres used do not have any temperature-dependent properties. Materials of this type can be heated to above the melting point of the matrix material and can be formed without any temperature dependent change in the properties of the reinforcing fibres.

Integrating SRCs in an injection molding process is attractive from the process engineering terms, since this makes it possible use the good mechanical strength and stiffness of the SRCs together with the geometric freedoms of the injection molding process. Stiffening ribs or functional elements can be combined with SRCs and final contours can be molded onto them. This is already state-of-the-art for materials reinforced with foreign fibres (Aurrekoetxea et al. 2006; Cabrera et al. 2004; Ries 2021), but this technique cannot be directly transferred to SRCs.

SRCs undergo a shrinkage process when heated (Le Bozec et al. 2000). This takes place on account of the retarding fibres and is the reason why SRCs must be fixed in a clamping frame during forming processes (Cabrera et al. 2004). This makes the integration of SRCs into an injection molding process with simultaneous forming and molding on final contour almost impossible and requires a different process engineering solution. The mold contour can be produced before by thermoforming and integrated in the injection molding process. Considering the process chain required to achieve the finished contour, this seems to be uneconomical. Despite this, a number of groups are conducting research in this area (Andrzejewski et al. 2018; Aurrekoetxea et al. 2006; Jerpdal et al. 2020). Jerpdal et al. (2020) researched the influence of back injection on the mechanical properties of an already compacted SRC based on PET. They overmolded SRCs of different thicknesses with incompatible plastic melt, removed this, and investigated the mechanical properties of the composites.

All the investigations conducted so far have been on consolidated SRCs. To simplify the process chain, a combination of the direct forming process (Paßmann 2009; Ries 2015) and back injection would seem logical. During the direct forming process, the fabric layers are stacked and placed in a heatable mold. Forming takes place prior to consolidation of the fabric layers, thus making it possible to get by without the process step of prior consolidation. If the fabric layers are heated under pressure, it is possible to dispense with the clamping frame, thus permitting integration in the injection molding process.

For this combined compaction and back-injection process, the fabric layers are stacked in the injection mold, a compacting force is applied, and the fabric layers are

compacted under heat and pressure. During compaction, the melt is injected into the cavity. Inside the cavity, the fabric layers are not consolidated by the compacting force but solely through the pressure of the melt. Previous investigations have shown that the adhesion achieved depends to a large extent on the temperature of the melt. With a barrel wall temperature of 280 °C, forces of 5.43 MPa were determined in a shear test. Measurements of the local pressure and temperature levels inside of the cavity showed that these can be readily controlled via the machine parameters. In addition, using the data captured by the temperature sensors in the mold, it was shown that, due to the onset of cooling, the time at which injection takes place has a major influence on the temperature of the mold at the time of injection, but this has little effect on adhesion (Jakob et al. 2021).

An improvement in adhesion linked to the temperature of the melt can lead to a decrease in the mechanical strength of the SRCs. An excessively high temperature melts the oriented crystalline structure and results in the loss of self-reinforcement.

This paper sets out to examine the influence of the process on the mechanical properties of the composites. In order to investigate the mechanical properties of back-injected SRCs, it is necessary to remove the injected part in the back-injected area. To make this possible, the SRCs were back-injected with an incompatible polymer (POM) where adhesion to the SRCs will not occur. This can be removed from the SRCs after overmolding. The SRCs are then influenced by the pressure and temperature of the melt, but the measurement of the mechanical properties of the SRCs can be performed as a function of the process parameters without being influenced by a change of thickness in cross-section. The compaction achieved in the SRCs and thus, the thickness of SRC in the compacted area, is analysed by microscopy and the findings are linked to mechanical properties.

2 Experimental studies

2.1 Materials

2.1.1 SRC – Torodon®: Torodon® from Don&Low, Forfar, United Kingdom, was the material used for the hot compaction. This is made of 100% polypropylene and SRCs made of this plain weave textile are specified with a strength of 180 MPa, a stiffness of 4350 MPa, an elongation at break of 11% and a density of 0.9 g/cm³. This is a fabric that is made of tapes specially for hot compaction and has co-extruded edge layers. The processing window for hot compaction is given as 120–140 °C.

2.1.2 POM – Hostaform® C 13031: The POM used is from Celanese, Sulzbach, Germany. It has an MFR of 1.4 g/min (190 °C, 2.16 kg), a density of 1.41 g/cm³, a tensile strength of 68 MPa and an elastic modulus of 3050 MPa. The material is used in injection molding for technical applications.

2.2 Processing

The tests were conducted on a specially developed tool which has heatable plates with a cavity on the sprue side and thus combines the function of a press and an injection mold. The tool is heated with 32 heating cartridges and has an overall heating power of 25.6 kW. It is cooled by direct water cooling. As shown in Figure 1, the mold has three temperature and pressure sensors in the cavity for measuring local pressures and temperatures.

The front platen is insulated from the clamping platens to achieve the best possible heating rates. The tool attains a heating rate of approx. 10 K/min and a cooling rate of approx. 100 K/min. Inside the clamping plates a second separate water-cooling system is applied to eliminate the heat that is introduced. A precise description of the tool can be found in (Jakob et al. 2021).

In injection molding processes, a large number of parameters can be modified. In order to modify the temperature and pressure in the back-molded area, specific parameters were chosen. These are set out in Table 1.

Six layers of the Torodon® fabric were used for the experiments. The processing was performed on an Arburg 470S injection molding machine. The tool was heated to the compaction temperature for the

process, the melt metered, and the layers of fabric placed between the press platens of the tool. The fabric layers were held at the compaction temperature for 60 s, regardless of the time at which the melt was injected. Injection was performed either within the 60 s holding time or after the start of cooling. The tool is cooled over a period of 150 s to ensure the dimensional stability of the composites. Figure 2 shows a schematically time-dependent plot of the tool temperature, the tool pressure and the in-mold pressure. The in-mold pressure curve is shifted for different times of injection. The point in time at which the melt is injected is always given in relation to the start of cooling, which is why the time of injection can also be negative. A more detailed explanation of the parameters and the relationship between temperature and pressure curves can be found in Jakob et al. (2021).

To enable the influence of the back injection on the composite to be measured, use was made of a polymer that was incompatible with the composite and hence did not bond to the SRC, as mentioned before. By using this incompatible polymer POM, it is possible to apply standardised test procedures to the specimen and to draw comparisons with SRCs consolidated in the conventional way by means of compaction pressure by a tool. If the injection-molded specimen would not be removed, the effect on the mechanical performance of the SRC in the back-injected area, brought by the influence of the melt temperature and pressure, would always be eliminated because of a simultaneous increase in cross-sectional area by the injected polymer. The method used here allows the back-injected polymer to be removed from the SRCs after processing, enabling a test to be conducted on the pure SRCs without any unwanted influence of the specimen geometry.

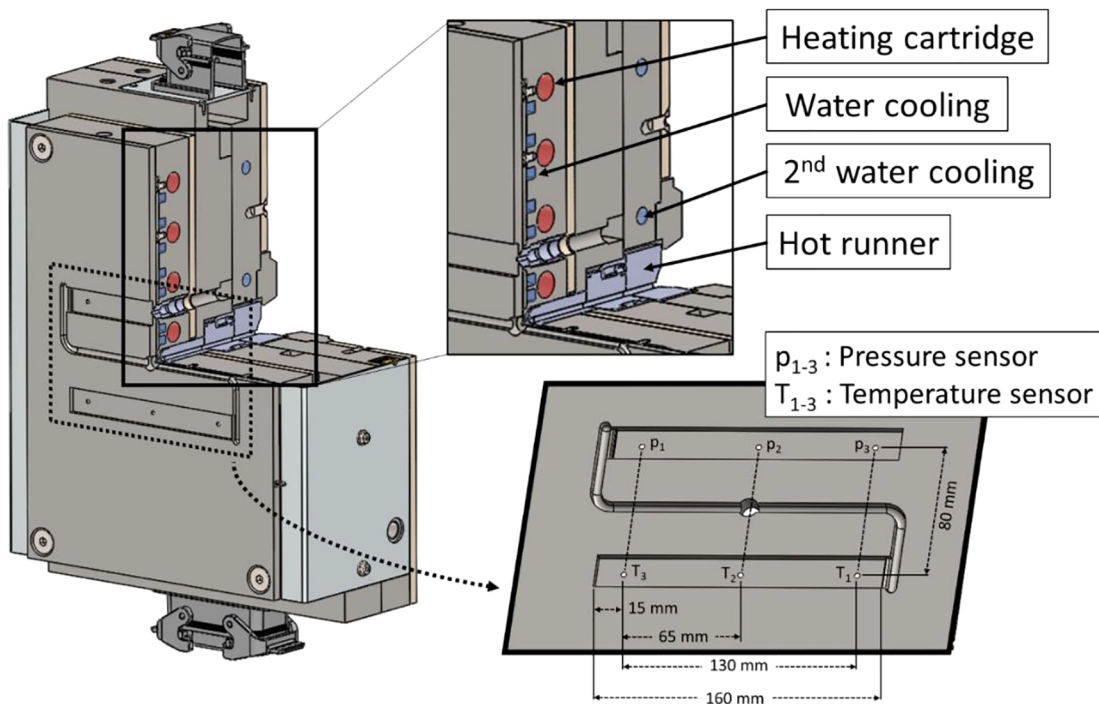
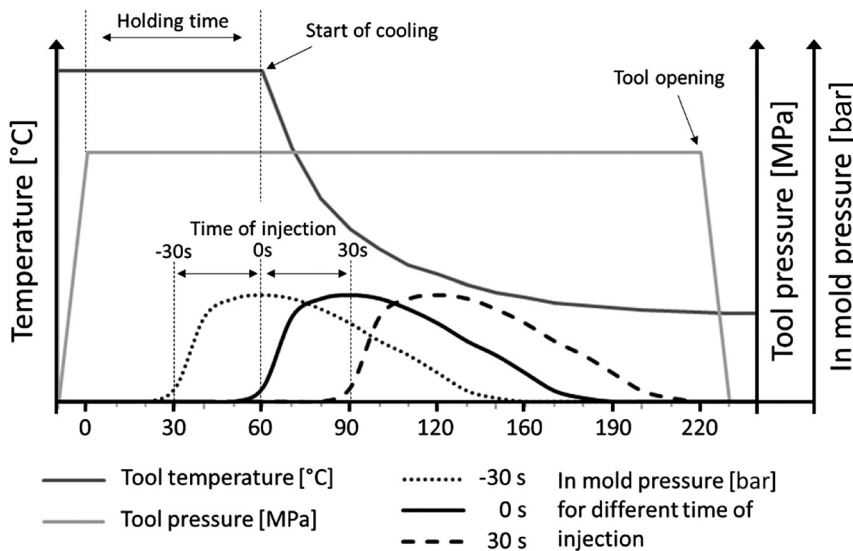


Figure 1: Tool for the combined compaction and back-injection process on the sprue side with the position of the internal temperature and pressure sensors.

Table 1: Process parameters for the combined compaction and back-injection process.

Varied Parameter					
Barrel temperature	[°C]	180	230	280	
Holding pressure	[bar]	200	250	300	
Time of injection	[s]	-30	-10	10	30

Constant parameter		
Injection speed	[cm ³ /s]	3
Compaction pressure	[MPa]	7
Compaction temperature	[°C]	130
Hot runner	[°C]	180
Cooling time	[s]	150
Second cooling	[°C]	45
Dosing speed	[mm/s]	150
Back pressure	[bar]	25

**Figure 2:** Schematic illustration of the time-dependent process temperature, tool pressure and in-mold pressure of the combined compaction and back-injection process.

2.3 Preparation

To determine the mechanical properties, tensile and bending test specimens were taken from the back-injected composites. Preparation was performed at three different points along the flow path, in the position of the sensors. The removal points for the tensile and bending test specimens and the dimensions of the individual specimens are shown in Figure 3. The specimens are prepared orthogonal to the direction of flow, so that the back-injected area with a width of 20 mm lies longitudinally on the specimens.

The specimens were prepared on a CNC-controlled specimen milling machine from Coesfeld, Dortmund, Germany. The overall length of the specimens is limited to 70 mm due to the geometry of the back-injected area. For the tensile test specimens, the parallel milled length in the tapered area was set at 24 mm so that the back-injected area is fully contained within this. As can be seen, the specimens were prepared in such a way that the back-injected area is in the centre of each specimen.

For the microscopic investigations, the specimens were removed at 25 mm from the gate (D_G) and observed in the direction of flow. Preparation was performed using a Leica Microtome, Nussloch, Germany. The specimens were first ground flat in a wet grinding process and then cut with the microtome. The specimen was observed in direct

reflected light using a digital microscope from Keyence, Neu-Isenburg, Germany.

2.4 Measuring

The tensile tests were carried out on a testing machine from Zwick und Roell, Ulm, Germany. A load cell for 10 kN and a free clamping length of 50 mm were used for the test. The elastic modulus was measured using a fine strain extensometer (model MultiXtens) system from Zwick und Roell. The measuring length for the fine strain extensometer was set at 24 mm. The elastic modulus was determined at 1 mm/min before switching over to a test speed of 5 mm/min. The maximum strength and the elongation at break were determined in addition to the elastic modulus.

The bending tests were also performed on the testing machine from Zwick and Roell. A three-point bending fixture with a support spacing of 40 mm and a 200 N load cell was used. The test speed for determining the elastic modulus was set at 5 mm/min before switching to a test speed of 20 mm/min. The radius of the supporting pins and of the compression die is 5 mm in each case. The test was carried out up to a maximum deflection of 4%. The strain was consistently measured with the machine's fine strain extensometer system. The bending stiffness and maximum strength of the specimens were determined.

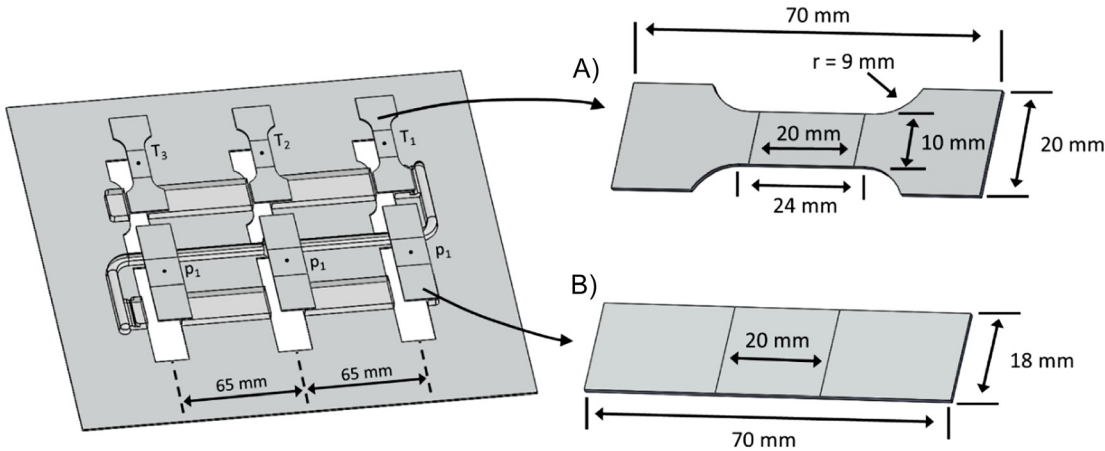


Figure 3: Position of the specimens used for the bending and tensile test with their geometric parameters, A) tensile test specimen, B) bending test specimen.

The back-injected side of the specimens was always positioned facing downward in the test setup.

The measurement of the temperature and pressure data was performed via Type K temperature sensors and quartz pressure sensors (Kistler, Winterthur, Switzerland) inside the tool. By evaluating the sensors, it is possible to detect the tool wall temperature and the cavity pressure. The tool wall temperature sensors also make it possible to determine the speed of the melt front. The data captured by the sensors and their evaluation is shown as an example in Figure 4. Figure 4A shows the curves recorded by the three temperature sensors over the flow path. The mean flow front velocity shown here is determined from the time lag between the melt coming into contact with Sensor 2 and Sensor 3.

For the evaluation of the sensor data, the mold wall temperature at the time of injection (T_i) is determined. A temperature increase (ΔT) subsequently occurs through the contact with the melt. With a constant tool temperature, this will be a function of the melt temperature. The pressure curve shown here is used to capture the maximum applied pressure ($\max \rho$) in the cavity and the tool wall temperature at the time of $\max \rho$ ($t_{\max \rho}$). A more precise description of the recorded

data and the influence on the tool wall temperature and the cavity pressure can be found in Jakob et al. (2021).

JMP®Pro Version 15.0.0 (SAS Institute GmbH, Heidelberg, Germany) was used to compile the regression models, which were drawn up using the ordinary least squares (OLS) method. In addition to the main effects, simple interaction effects and quadratic effects were included and examined in the model. The individual factors of the regression model are evaluated with the aid of a significance test (p value of 0.05). Non-significant factors are iteratively removed from the regression model. To identify possible outliers in the experimental plan, the residuals are examined in a t -distribution test and residuals outside the 95% limit are eliminated.

The model quality is evaluated on the basis of the coefficient of determination R^2 . This is calculated from the sum of squares (SS) of the residuals. The coefficient of determination assumes values between 0 and 1, where 1 indicates that 100% of the observations are explained by the model (Ronniger 2014). In addition to the coefficient of determination R^2 , the adjusted coefficient of determination R_{adj}^2 is specified. When calculating R_{adj}^2 , the degrees of freedom (DF) are taken into account so as to prevent any overfitting of the model. Also, the relative

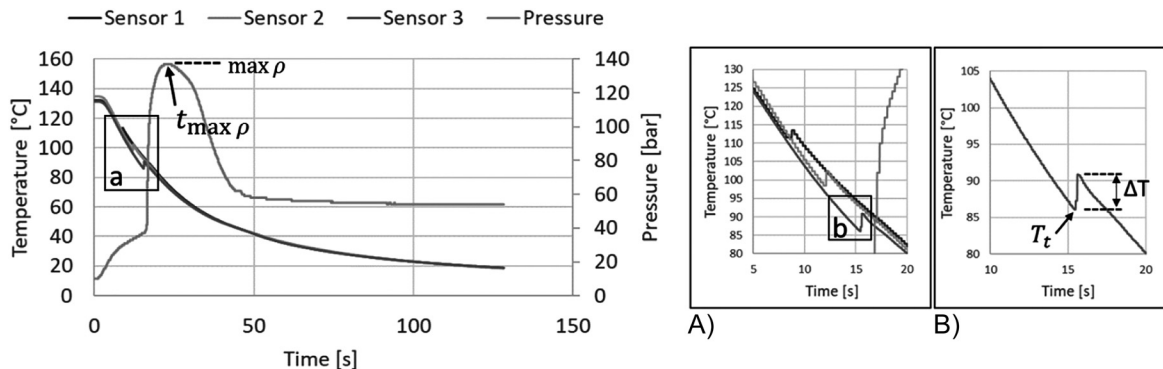


Figure 4: Temperature and pressure curves of the inner sensors (Jakob et al. 2021).

standard deviation, or root mean squared error (RMSE), is calculated for the respective model.

3 Results and discussion

3.1 Tensile tests

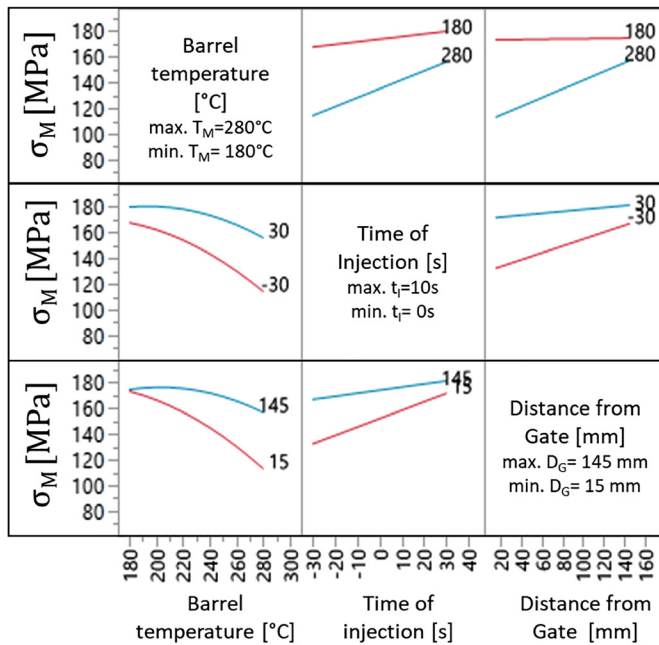
The influence of the machine parameters on the mechanical characteristic values of tensile strength (MPa) (σ_M) and elastic modulus (MPa) (E_M) was investigated. The investigations showed that barrel temperature, time of injection and distance from the gate have a significant influence on the strength of the SRCs. As shown in Figure 5, the strength decreases with an increasing barrel temperature. This is particularly clear for $t_I = -30$ s, where the strength of the SRCs falls from 170 MPa at 180 °C to 110 MPa at 280 °C. It is also evident that this effect is less pronounced for $t_I = 30$ s. In this case, the strength falls from 180 MPa at 180 °C to 160 MPa at 280 °C.

The correlation between decreasing strength and a rising compaction temperature is well known from the parameter effects in hot compaction (Biermann et al. 2015; Heim et al. 2012, 2013; Ronniger 2014). It is also shown that the time of injection causes a lower loss of strength the later the melt is injected. The tool temperature falls at the start of cooling, leading to a lower maximum temperature

in the SRCs upon contact with the melt, due to the lower temperature of the SRC (Jakob et al. 2021). The distance from the gate has a positive effect on the strength of the SRCs with an increasing distance. It is also clear that interaction effects exist between T_B and t_I as well as between T_B and D_G , and t_I and D_G . The interaction effects between T_B and t_I and between T_B and D_G are antagonistic, while the interaction effect between t_I and D_G is synergistic.

The investigation of the elastic modulus showed that barrel temperature, holding pressure and distance from the gate machine parameters have a significant effect. The elastic modulus falls with a rising barrel temperature and holding pressure but increases with the distance from the gate. As can be seen in Figure 6, antagonistic interactions exist between the holding pressure and the distance from the gate. It is also clear that the lower the holding pressure and the greater the distance from the gate, the smaller this interaction effect will be.

Similar effects can be observed for SRCs during hot compaction. Here too, the loss of stiffness is attributed to the influence of temperature during hot compaction (Biermann et al. 2015; Ries 2015) and the partial relaxation of the molecular chains (Alcock 2004; Menges et al. 2011). The regression model for \hat{E}_M shown here, however, with a model accuracy of $r^2 \approx 0.7$ still displays a high unidentified residual scatter, which is why the general



r^2 0.8683
 r^2_{adj} 0.857941
 RMSE 9.097594
 mean 158.6911
 DF 97

Regression model for $\hat{\sigma}_M$ [MPa]:

$$\begin{aligned}
 & -0.3677 \cdot T_B + 0.4404 \cdot t_I + 0.1671 \cdot D_G \\
 & - (T_B - 230) \cdot (T_B - 230) \cdot 0.0033 \\
 & + (T_B - 230) \cdot (t_I \cdot 0.0049) \\
 & + (T_B - 230) \cdot (D_G - 80) \cdot 0.0033 \\
 & - t_I \cdot (D_G - 80) \cdot 0.0032 \\
 & + 233.5308 + \varepsilon
 \end{aligned}$$

$T_B =$ Barrel temperature [°C]
 $t_I =$ Time of injection [s]
 $D_G =$ Distance from gate [mm]
 $\varepsilon =$ Model error [-]

Figure 5: Interaction plots for the regression model of estimated tensile strength ($\hat{\sigma}_M$) built with data from the tensile tests.

statement of the regression model has to be evaluated critically.

To create a reference for the tests, two further SRCs were produced, prepared and tested. One specimen was prepared with the same compacting parameters as the experimental plan but was not back-injected (Ref_{not Inj.}). This makes it possible to record the influence on the fabric layers through heating without pressure. A further reference specimen was compacted with two plates without a cavity (Ref_{Comp.}) to compare the properties of a conventionally consolidated SRC. Figure 7 shows all the specimens in the experimental plan on a scatter plot with the reference specimens marked separately. The determination of the tensile strength shows that both Ref_{not Inj.} and Ref_{Comp.} are in the upper range of the measured values. When the elastic modulus is determined, however, this shows widely scattered characteristic values for Ref_{not Inj.} which are located more in the middle range of the test series, while Ref_{Comp.} was measured at the upper limit of the test series for the elastic modulus.

The tapes retain their mechanical strength due to the lower temperature in the tool of 130 °C for the two reference specimens. In the case of Ref_{not Inj.} a lower stiffness is seen with a high strength, despite the low temperature exposure. This is attributable to insufficient consolidation of the tapes, which, under load, initially behave like a textile rather than like a composite.

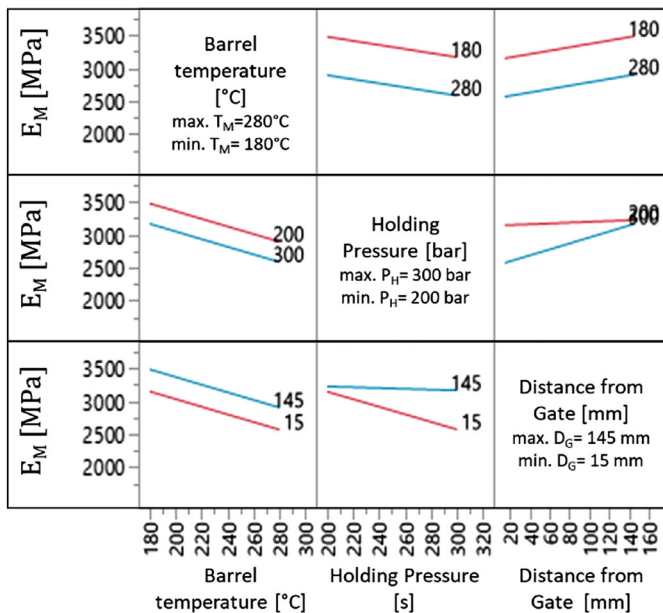
The reference values determined lie within the characteristic values recorded in the test series. It is thus

possible to adjust them via the suitable machine parameters. Since the tapes have their highest strength in the non-consolidated state, the characteristic values from the tensile tests are not suitable for the evaluation of the consolidation of the composites, since the strength decreases steadily with increasing compaction temperature (Alcock 2004; Ries 2015). Bending tests provide more information here, since they allow an evaluation of the adhesion of the tapes to each other in the SRC.

3.2 Bending tests

The results of the bending tests were evaluated with the same software as for the tensile tests. The parameters flexural strength (σ_{fM}) and flexural stiffness (E_f) were investigated and the corresponding regression models drawn up. The regression model build for σ_{fM} is shown in Figure 8.

This shows a decreasing flexural strength for a rising barrel temperature, corresponding to the interactions already observed for the tensile strength (Figure 5). Upon closer observation, a parabolic curve with a peak at approx. 220 °C is seen for the strength over the barrel temperature at $t_f = 30$ s and for $D_G = 145$ mm. The strength at $T_B = 180$ °C is also seen to decrease with a later t_f , while the opposite effect is evident for $T_B = 280$ °C. This effect indicates insufficient consolidation of the tapes for the combination of $T_B = 180$ °C, $t_f = 30$ s and $D_G = 145$ mm. For



r^2 0.704485
 r^2_{adj} 0.690579
 RMSE 210.429
 mean 3040.806
 DF 90

Regression model for \hat{E}_M [MPa]:

$$-5.7889 \cdot T_B - 3.0213 \cdot P_H + 2.6265 \cdot D_G + (P_H - 250) \cdot (D_G - 80) \cdot 0.0394 + 4904.691 + \varepsilon$$

$T_B =$ Barrel temperature [°C]
 $P_H =$ Holding Pressure [bar]
 $D_G =$ Distance from gate [mm]
 $\varepsilon =$ Model error [-]

Figure 6: Interaction plots for the regression model of the estimated elastic modulus (\hat{E}_M) built with data from the tensile tests.

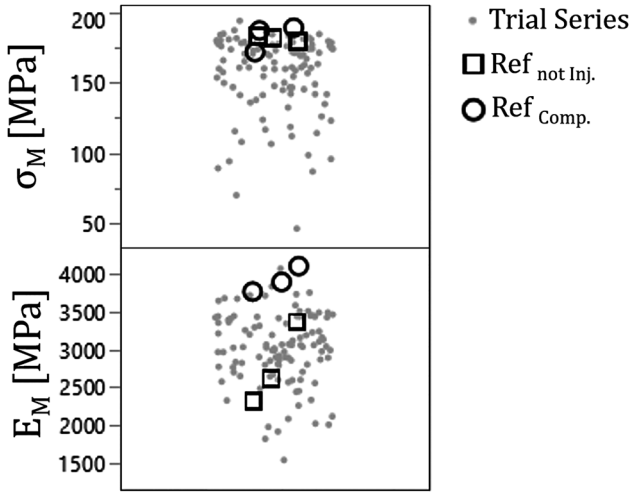


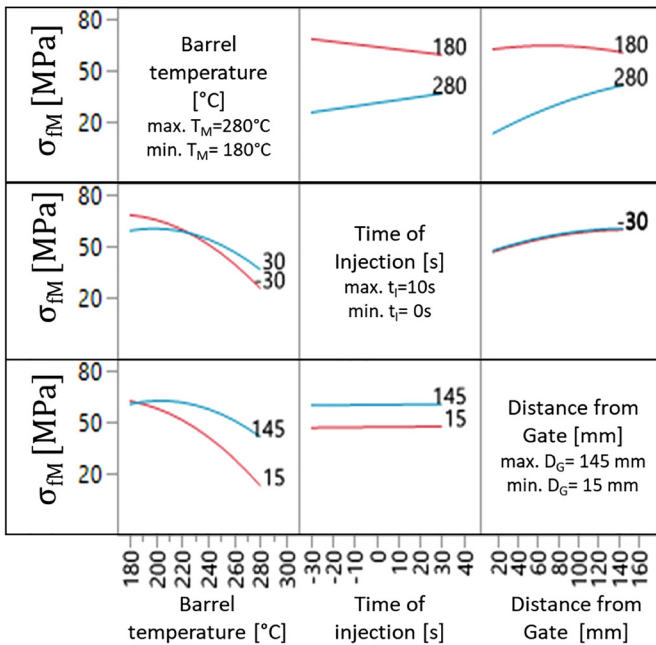
Figure 7: Scatter plot of the tensile test trial series with characteristic values of Ref_{not Inj.} and Ref_{Comp.}.

$T_B = 280 \text{ }^\circ\text{C}$, a clear increase in strength with increasing D_G is observed. The evaluation of \hat{E}_f shows a similar effect as shown in Figure 9.

For \hat{E}_f too, a parabolic curve is seen over T_B for $t_I = 30$ and $D_G = 145$, with a peak at $220 \text{ }^\circ\text{C}$, and this similarly indicates insufficient consolidation. For $T_B = 280 \text{ }^\circ\text{C}$, a clear increase in stiffness can also be observed with increasing t_I and D_G . This is due to the tapes being thermally damaged through melting.

With an increasing t_I , the mold temperature drops considerably after the start of cooling. The slow injection speed of approx. 18–19 mm/s means that the tool cools down by up to $26 \text{ }^\circ\text{C}$ for the given cooling ramp during the time it takes for the melt front to move from position 1 to position 3 (see Figure 1) (Jakob et al. 2021). The compaction temperature of the tool means that the coextruded edge layers have already melted prior to contact with the injected melt. Since the holding pressure is statistically not a significant influencing factor, it can be assumed that even a low contact pressure for the tapes will be sufficient to bond them if the temperature is high enough. Upon contact with the injected melt, the temperature of the SRCs rises. The temperature attained will depend on the temperature of the SRCs and the temperature of the melt. The temperature of the SRCs was not varied directly. Since t_I was varied, however, this leads to different tool temperatures and hence to different temperatures in the SRCs too at the time of injection.

For a late t_I and a long D_G it can be assumed that the SRCs will cool down to below the temperature required for adhesion without having had sufficient contact with the melt and thus, no pressure. In addition, with a low T_M the melt temperature is not high enough to reheat the SRCs sufficiently to cause adhesion between the fabric layers. These conditions, which lead to poor adhesion, occur, for example, at $t_I = 30$, $D_G = 145$ and a melt temperature below $220 \text{ }^\circ\text{C}$.



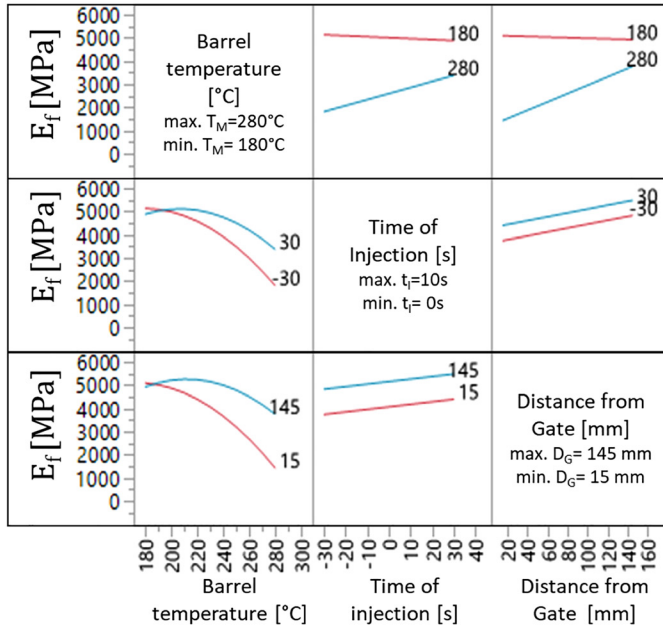
r^2 0.954759
 r^2_{adj} 0.951565
 RMSE 3.646342
 mean 49.07832
 DF 92

Regression model for $\hat{\sigma}_{fM}$ [MPa]:

$$\begin{aligned}
 & -0.3344 \cdot T_B + 0.0131 \cdot t_I + 0.0996 \cdot D_G \\
 & - (T_B - 230) \cdot (T_B - 230) \cdot 0.0036 \\
 & + (T_B - 230) \cdot t_I \cdot 0.0033 \\
 & + (T_B - 230) \cdot (D_G - 80) \cdot 0.0023 \\
 & - (D_G - 80) \cdot (D_G - 80) \cdot 0.0007 \\
 & + 125.457 + \varepsilon
 \end{aligned}$$

$T_B = \text{Barrel temperature } [^\circ\text{C}]$
 $t_I = \text{Time of injection } [s]$
 $D_G = \text{Distance from gate } [mm]$
 $\varepsilon = \text{Model error } [-]$

Figure 8: Interaction plots for the regression model of estimated flexural strength ($\hat{\sigma}_{fM}$) built with data from the bending tests.



r^2 0.907201
 r^2_{adj} 0.901278
 RMSE 426.9358
 mean 4059.279
 DF 101

Regression model for \hat{E}_f [MPa]:

$$\begin{aligned}
 & -23.741 \cdot T_B + 10.7686 \cdot t_I + 8.2203 \cdot D_G \\
 & - (T_B - 230) \cdot (T_B - 230) \cdot 0.3237 \\
 & + (T_B - 230) \cdot t_I \cdot 0.3022 \\
 & + (T_B - 230) \cdot (D_G - 80) \cdot 0.1921 \\
 & + 9415.2410
 \end{aligned}$$

T_B = Barrel temperature [°C]
 t_I = Time of injection [s]
 D_G = Distance from gate [mm]
 ε = Model error [-]

Figure 9: Interaction plots for the regression model of estimated flexural strength (\hat{E}_f) built with data from the bending tests.

Reference plates were also made for the bending tests in the same way as for the previous tensile tests. A reference was once again produced with the same parameters as for the tensile test series, which was not back-injected (Ref_{not Inj.}). A further reference was fabricated between two plates without a cavity (Ref_{Comp.}). The results are shown in Figure 10.

When evaluating the reference data for the bending tests it is seen that the strength and stiffness of Ref_{Comp.} are within the test series. The same mechanical properties of the SRCs can thus be adjusted within the test series via injection molding. The results for Ref_{not Inj.} show that the strength of the SRCs is in the lower range of the measured values. At the same time, however, the measured stiffness is in the upper range, approaching the measured stiffness of Ref_{Comp.}. Based on the determined stiffness, it can be assumed that there is at least partial adhesion between the fabric layers. The low flexural strengths seem to prove that bonds are not very stable, and that the layers are separated again with increased bending of the specimens.

3.3 Microscopy

In order to assess how the consolidation of the SRCs is conditioned by the process parameters, microscopy images were taken of selected samples from the test series.

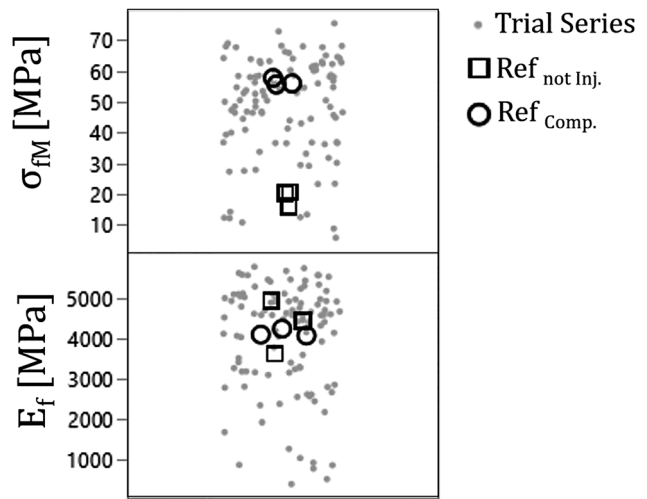


Figure 10: Scatter plot of the bending test trial series with characteristic values of Ref_{not Inj.} and Ref_{Comp.}.

Figure 11 shows images of the transition area on SRCs back-injected with POM and produced with different process parameters. It is clear that the thickness of the SRCs in the consolidation area achieved through the tool pressure is higher than for the consolidation area achieved through the melt pressure, which means that the SRCs are compacted to a greater extent in the area subjected to melt pressure.

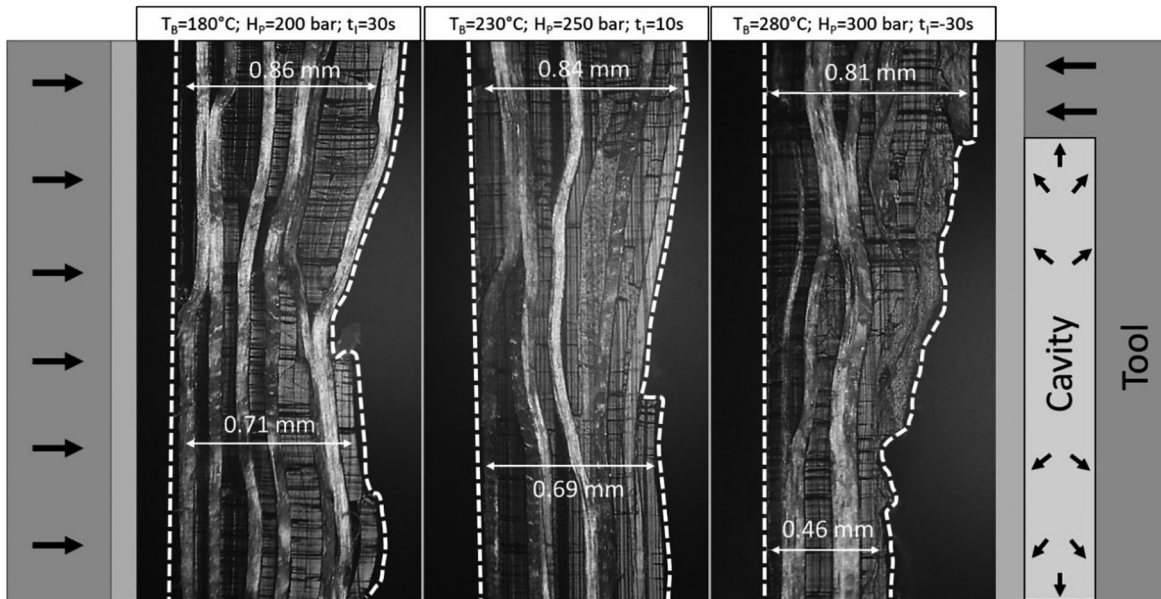


Figure 11: Microscopy images of SRCs back-injected with POM at the transition between compaction via the tool and compaction via the pressure of the injected polymer – all samples are prepared at $D_G = 25\text{--}30$ mm.

As expected, this effect is greatest at $T_B = 280$ °C and $t_i = -30$ s. Since the holding pressure has no significant influence on the mechanical properties of the SRCs, as the regression model has shown, it can be assumed that the effect observed is due to T_B and t_i . The fabric layers are completely melted in some cases if the temperatures are excessively high, and the thickness of the SRC is considerably reduced. From this, it is also possible to explain the changes in the previously determined strengths and stiffnesses of the SRCs via the parameters. D_G is also expected to have an influence on the thickness that results in the SRCs, but this was not taken into account in the microscopy analyses. The thickness of the SRCs is lower in the back-injected areas, and this would seem to be true for all the parameters investigated here. If the surface pressure in the area by the press plate (7 MPa) is compared with the surface pressure in the back-injected area (20 MPa), this correlation would seem plausible.

4 Conclusions

This work examines the influence of selected process parameters on the tensile and flexural strengths of SRCs made up of six layers of Torodon® in a combined compaction and back-injection process. The barrel temperature, holding pressure and time of injection were varied for the tests. In addition, test specimens were taken from different areas of the specimens in order to determine the influence of the distance from the gate.

The mechanical characteristic values determined from the tensile and bending tests indicate that the properties obtained through the combined compaction and back-injection process are dependent to a great extent on the selected parameters. With a barrel temperature of 180 °C, employing the earliest possible time of injection will be advantageous for achieving an optimum flexural strength, while with a barrel wall temperature of 280 °C an early time of injection will lead to thermal loss of the self-reinforcement in the SRCs already. From the results, it is possible to conclude that the bending tests performed permit a better assessment of the adhesion within the composite and hence a fundamental evaluation of the consolidation. Tensile tests, by contrast, only detect the thermal gradation over the maximum strength and stiffness of the SRCs.

The microscopy images show the clear melting of individual fabric layers with a high barrel temperature and a time of injection of -30 s. The thickness in the back-injected area of the SRCs is then reduced by 57%. The clear thermal degradation is also reflected in the mechanical properties.

In principle, however, it was possible to consolidate the fabric layers via the melt in the combined compaction and back-injection process. A comparison of the mechanical properties of the SRC consolidated via the melt with those of a conventionally consolidated SRC shows that, within the parameter range investigated here, it is possible to set the mechanical characteristic values at the same level. The POM material used for back injection has a higher heat capacity

and a viscosity that differs from PP. The values determined here cannot therefore be directly transferred to PP, but the qualitative correlation is identical. A comparison of the sensors inside the tool (see Figure 4) shows that ΔT is an average of 1.1 °C (13.6%) higher for POM. The cavity pressure is also higher (43.5 bar, 24.0%) when POM is used. The melt front speed, by contrast, is nearly unchanged, with an increase of 0.12 mm/s (0.6%). Further polymers should be investigated for back injection so as to permit a better estimate to be made.

Author contributions: All the authors have accepted responsibility for the entire content of this submitted manuscript and approved submission.

Research funding: None declared.

Conflict of interest statement: The authors declare no conflicts of interest regarding this article.

References

- Alcock, B. (2004). *Single polymer composites based on polypropylene: processing and properties*, Doctoral dissertation. Queen Mary University of London, London.
- Andrzejewski, J., Przystarczykowski, P., and Szostak, M. (2018). Development and characterization of poly(ethylene terephthalate) based injection molded self-reinforced composites. Direct reinforcement by overmolding the composite inserts. *Mater. Des.* 153: 273–286, <https://doi.org/10.1016/j.matdes.2018.04.084>.
- Aurrekoetxea, J., Castillo, G., Cortes, F., Sarrionandia, M.A., and Urrutibeascoa, I. (2006). Failure of multimaterial fusion bonding interface generated during over-injection molding/thermoforming hybrid process. *J. Appl. Polym. Sci.* 102: 261–265, <https://doi.org/10.1002/app.23696>.
- Biermann, D., Gausemeier, J., Heim, H.-P., Hess, S., Peters, G., Ries, A., and Wagner, T. (2015). Planning and optimisation of manufacturing process chains for functionally graded components—part 2: case study on self-reinforced thermoplastic composites. *Prod. Eng. Res. Devel.* 9: 405–416, <https://doi.org/10.1007/s11740-015-0610-2>.
- Le Bozec, Y., Kaang, S., Hine, P., and Ward, I. (2000). The thermal-expansion behaviour of hot-compacted polypropylene and polyethylene composites. *Compos. Sci. Technol.* 60: 333–344, [https://doi.org/10.1016/S0266-3538\(99\)00129-3](https://doi.org/10.1016/S0266-3538(99)00129-3).
- Cabrera, N., Alcock, B., Loos, J., and Peijs, T. (2004). Processing of all-polypropylene composites for ultimate recyclability. *P I MECH ENG L-J MAT* 218: 145–155, <https://doi.org/10.1177/146442070421800208>.
- Cherif, C. (2011). *Textile Werkstoffe für den Leichtbau*. Springer, Berlin Heidelberg.
- Heim, H.-P., Biermann, D., and Maier, H. (Eds.). (2012). *1st International conference on thermo-mechanically graded materials*. Verlag Wissenschaftliche Scripten, Auerbach.
- Heim, H.-P., Biermann, D., and Homberg, W. (Eds.). (2013). *Functionally graded materials in industrial mass production*, Vol. 2. Verlag Wissenschaftliche Scripten, Auerbach.
- Hine, P., Ward, I., Olley, R., and Bassett, D. (1993). The hot compaction of high modulus melt-spun polyethylene fibres. *J. Mater. Sci.* 28: 316–324, <https://doi.org/10.1007/BF00357801>.
- Hine, P., Ward, I., and Teckoe, J. (1998). The hot compaction of woven polypropylene tapes. *J. Mater. Sci.* 33: 2725–2733, <https://doi.org/10.1023/A:1017540530295>.
- Hine, P., Ward, I., Jordan, N., Olley, R., and Bassett, D. (2003). The hot compaction behaviour of woven oriented polypropylene fibres and tapes. I. Mechanical properties. *Polymer* 44: 1117–1131, [https://doi.org/10.1016/S0032-3861\(02\)00809-1](https://doi.org/10.1016/S0032-3861(02)00809-1).
- Jakob, F., Pollmeier, J., and Heim, H.-P. (2021). Process influences in the combined compacting and back-injection process to produce back-injected self-reinforced composites (SRCs) – analysis via multiple regression modelling. *Int. Polym. Proc.* 36: 608–619.
- Jerpdal, L., Schuette, P., Ståhlberg, D., and Åkermo, M. (2020). Influence of temperature during overmolding on the tensile modulus of self-reinforced poly(ethylene terephthalate) insert. *J. Appl. Polym. Sci.* 137: 48334, <https://doi.org/10.1002/app.48334>.
- Jordan, N., Bassett, D., Olley, R., Hine, P., and Ward, I. (2003). The hot compaction behaviour of woven oriented polypropylene fibres and tapes. II. Morphology of cloths before and after compaction. *Polymer* 44: 1133–1143.
- Menges, G., Haberstroh, E., Michaeli, W., and Schmachtenberg, E. (2011). *Menges Werkstoffkunde Kunststoffe*, 6th ed. Carl Hanser Verlag, Munich.
- Olley, R., Bassett, D., Hine, P., and Ward, I. (1993). Morphology of compacted polyethylene fibres. *J. Mater. Sci.* 28: 1107–1112, <https://doi.org/10.1007/BF00400899>.
- Paßmann, D. (2009). *Prozessinduzierte Gradierung eigenverstärkter Polypropylen-Faserverbunde beim Heißkompaktieren und Umformen*, PPH ZAPOL Dmochowski. Sobczyk Spółka Jawna, Szczecin.
- Rasburn, J., Hine, P., Ward, I., Olley, R., Bassett, D., and Kabeel, M. (1995). The hot compaction of polyethylene terephthalate. *J. Mater. Sci.* 30: 615–622, <https://doi.org/10.1007/BF00356319>.
- Ries, A. (2015). *Thermo-mechanische Gradierung eigenverstärkter Polypropylen-Composite*. Kassel University Press, Kassel.
- Ries, A. (2021). Structural description of self-reinforced polypropylene composites. *J. Appl. Polym. Sci.* 138: e51215, <https://doi.org/10.1002/app.51215>.
- Ronniger, C.U. (2014). *Taschenbuch der statistischen Qualitäts- und Zuverlässigkeitsmethoden. Die wichtigsten Methoden und Verfahren für die Praxis*. CRGRAPH, Munich.